CILAMCE 2017

Florianópolis - Santa Catarina - Brazil

COUPLED HYDRO-MECHANICAL ANALYSIS OF HYDRAULIC FRACTURE IN NATURALLY FRACTURED RESERVOIRS USING FINITE ELEMENTS WITH EMBEDDED DISCONTINUITIES

Aura M. Zuleta

Leonardo Guimarães

Leila Beserra

Kewin Passos

amzuletago@unal.edu.co

leonardo@ufpe.br

leila.brunet@ufpe.br

kpassos@unal.edu.co

Department of Civil Engineering, Federal University of Pernambuco

R. Acadêmico Hélio Ramos, s/n, Cidade Universitária, 50740-530, Recife, PE, Brazil

Osvaldo Manzoli

omanzoli@feb.unesp.br

Department of Civil Engineering, State University of Sao Paulo

Univ. Estadual Paulista, 17033-360, Bauru-SP, Brazil

Abstract. *Modeling hydraulic fracturing become a challenge task when is necessary have a realistic knowledgement of some rock criteria. This paper show simulations concerning to hydraulic problem in naturally fractured reservoirs. A numerical code that includes strong discontinuities embedded in a finite element mesh was used to perform simulations of reservoirs that will be submit to hydraulic fracturing operations. The code allows obtaining results for fluid flow and propagation of fractures analysis using a coarse meshes and reasonable computational time. Some simulations were performed considering different scenarios for the initial stress strain. The presence of casing, natural fractures and the angle of perforating around wellbore were also considered. The analysis shows the increase of connectivity of natural fractures previously not connected as a result of induced fractures created by medium pressurization.*

Keywords: *Hydraulic Fracturing, Natural Fractures, Finite Elements, Embedded Discontinuities.*

INTRODUCTION

Hydraulic fracturing is a method widely used in petroleum industry to recover as much oil as possible from the reservoir. In this method, artificial fractures are induced by fluid injection in order to increase rock permeability. In a naturally fractured reservoir it is fundamental to know the influence of these fractures on the geometry of the induced fracture because this is decisive in the mechanical properties of the rock, in-situ stresses and local heterogeneity. Due to the strong coupling between fluid flow and mechanical behavior, the presence of weakness planes by the existing natural fractures, modeling hydraulic fracturing becomes a challenge task. The choice of an appropriate constitutive model that predict the mechanical behavior in a realistic way as well as takes into account the properties from the reservoir-rock system, such as fracture energy, is a critical point in modeling hydraulic fracturing.

The hydraulic fracturing problem in naturally fractured reservoirs was simulated in a numerical code that adopts a strong discontinuity approach to embed discontinuities in a finite element mesh, and provides a numerical fluid flow analysis in a deformable reservoir. The resulting code is used to model hydraulic fracture propagation in naturally fractured reservoirs with relatively coarse meshes and reasonable computational time. The hydro-mechanical coupling has been determined by a law that relates the variation of permeability as a function of the displacement jump from the mechanical problem.

In a classic case, the preferential direction of hydraulic fracture propagation is perpendicular at maximum principal stress because it represents the lowest work way and aperture of hydraulic fracture is in direction to minimum principal stress, but it is important in a naturally fractured reservoir have a detailed knowledge of propagation and aperture direction with the purpose of take decisions regarding the conditions under which the fracturing operation is going to be realize.

To evaluate the effect of initial stress state in the direction of the induced fractures, the simulations were performed considering different scenarios for the initial stress state. The analysis included the effect of pressurized medium in network interconnecting with fractures previously not connected.

1 MODEL FORMULATION

1.1 Strong discontinuity approach

A strong discontinuity approach was proposed by (Manzoli, 2011; Manzoli & Shing, 2006), to embed discontinuities into finite elements. The strong discontinuity approach was implemented in the in-house numerical code CODE_BRIGHT (Guimarães, Gens, & Olivella, 2007; Olivella, Gens, Carrera, & Alonso, 1996), which performs numerical analysis of fluid flow in a deformable reservoir.

The finite element formulation has fundamental aspects from discontinuity such as kinematics and static information. The kinematic enrichment must correctly reflect the position of the interface in the element as well as the relative displacement (opening and sliding) between the two opposite faces of the interface. Furthermore, the traction continuity condition must be properly imposed to ensure a correct relationship between the tractions in the internal interface and the stresses in the surrounding continuum portion (considered linearly elastic and isotropic).

Consider the triangular element with three nodes from domain Ωe, length le, with a band of strain localization Se, with k, which divides the element into two parts, isolating the node 1 from nodes 2 and 3 (Figure 1).

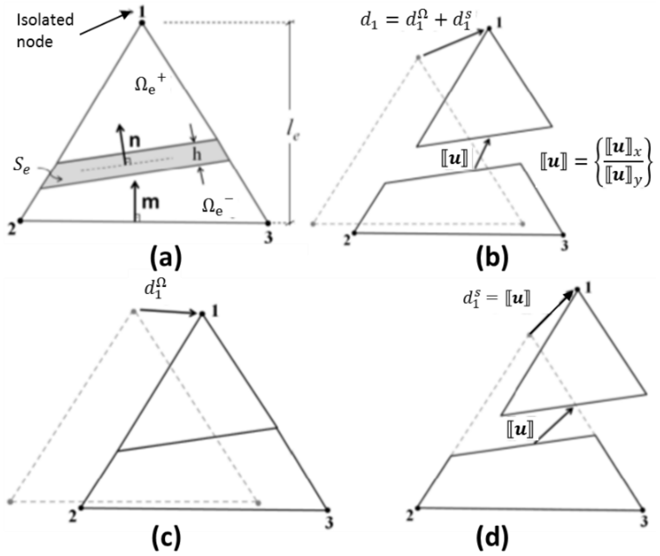

Figure 1.finite element crossed by a localization band (Beserra, 2015).

The displacement field jump, [[$\mathbf{u}$]], on S lead to a rigid-body relative motion, driving to the following nodal displacements:

$$d_1 = [[\boldsymbol{u}]]; d_2 = 0; d_3 = 0 \tag{1}$$

With finite element strain-displacement relationship will be obtained the deformation of continuum. i =1,2,3 represents the vector of nodal displacements of node i, due to the jump in the displacement field [[$\mathbf{u}$]].

$$\varepsilon = \sum_{i=1}^{3} \boldsymbol{B}_i(\boldsymbol{D}_i - \boldsymbol{d}_i) = \sum_{i=1}^{3} \boldsymbol{B}_i\boldsymbol{D}_i - \boldsymbol{B}_i[[\boldsymbol{u}]] \tag{2}$$

$$\varepsilon = \boldsymbol{BD} - \varepsilon^R$$

$\boldsymbol{D}_i$ is the nodal displacement vector and Bi is the standard finite element strain–displacement matrix. The deformation due to the displacement field jump can be written as

Proceedings of the XXXVIII Iberian Latin-American Congress on Computational Methods in Engineering
P.O. Faria, R.H. Lopez, L.F.F. Miguel, W.J.S. Gomes, M. Noronha (Editores), ABMEC, Florianópolis, SC, Brazil, November 5-8, 2017.

$$\begin{Bmatrix} \varepsilon_x^R \\ \varepsilon_y^R \\ \varepsilon_z^R \end{Bmatrix} = \frac{1}{l_e}\begin{bmatrix} m_x & 0 \\ 0 & m_y \\ m_y & m_z \end{bmatrix}\begin{Bmatrix} [[\boldsymbol{u}]]_x \\ [[\boldsymbol{u}]]_y \end{Bmatrix} = \frac{\boldsymbol{M}}{l_e}[[\boldsymbol{u}]] \tag{3}$$

Where **M** is a matrix containing the value of m (normal to the opposite side of the isolated node) components and le is the distance between the isolated node and the opposite side of the element.

The stress field is given by:

$$\sigma = \Sigma^c(\varepsilon) = \Sigma^c\left(\boldsymbol{BD} - \frac{\boldsymbol{M}}{l_e}[[\boldsymbol{u}]]\right) \tag{4}$$

where Σ^c is the material constitutive matrix of the continuum. The vector of internal forces corresponding to the finite element with area Ae, is given by:

$$\begin{aligned} f_{int} &= \int_{\Omega_e} \boldsymbol{B}^T \boldsymbol{\sigma} d\boldsymbol{\Omega}_e = \boldsymbol{B}^T \boldsymbol{\sigma} \boldsymbol{A}_e = \boldsymbol{B}^T \\ f_{int} &= \boldsymbol{B}^T \Sigma^c \left(\boldsymbol{BD} - \frac{M}{l_e}[[\boldsymbol{u}]]\right)\boldsymbol{A}_e \end{aligned} \tag{5}$$

The deformation and its corresponding stress in the localization band can be written as follows:

$$\varepsilon_s = \varepsilon + \frac{N}{k}[[\boldsymbol{u}]] = \boldsymbol{BD} - \frac{M}{l_e}[[\boldsymbol{u}]] + \frac{N}{k}[[\boldsymbol{u}]] \tag{6}$$

$$\sigma_s = \Sigma^s(\varepsilon_s) \tag{7}$$

where k, denotes the bandwidth of strain localization, Σ^s is the constitutive matrix of the discontinuity surface and. N is a matrix obtained from the components of the normal vector n (normal to the discontinuity), as:

$$\boldsymbol{N} = \begin{bmatrix} n_x | & 0 \\ 0 & | n_y \\ n_y | & n_x \end{bmatrix} \tag{8}$$

The surface forces in the region of localization band must be in equilibrium with the forces calculated in the surround (point in the continuous portion which borders the band):

$$\boldsymbol{N^T}(\boldsymbol{\sigma_s} - \boldsymbol{\sigma}) = \boldsymbol{0} \tag{9}$$

Replacing the Eq. (4) e (7) in (9):

$$\boldsymbol{N}^T \boldsymbol{\Sigma}^s \left(\boldsymbol{BD} - \frac{\boldsymbol{M}}{l_e}[[\boldsymbol{u}]] + \frac{\boldsymbol{N}}{k}[[\boldsymbol{u}]] \right) - \boldsymbol{N}^T \boldsymbol{\Sigma}^c \left(\boldsymbol{BD} - \frac{\boldsymbol{M}}{l_e}[[\boldsymbol{u}]] \right) = 0 \tag{10}$$

Solving the Eq. (10) will be obtained the displacement jump, $[[\mathbf{u}]]$. Since the jump components are determined, the stress tensor in the element can be obtained by Eq (4).

1.2 Variation law of permeability

The hydro-mechanical coupling has been determined by a law that relates the variation of permeability as a function of the displacement jump from the mechanical problem, as follow:

$$k_s = \frac{[[\boldsymbol{u}]]_n^2}{12} \tag{11}$$

where $[[\boldsymbol{u}]]_n$ is the normal jump aperture.

The numerical code, CODE_BRIGHT, uses the convergence criterion of Newton-Raphson, also it works with an IMPLEX algorithm (Oliver, Huespe, & Cante, 2008).

1.3 Damage model

The damage is the degradation of the material stiffness. The chosen model allows it to be calculated an effective damage stress.

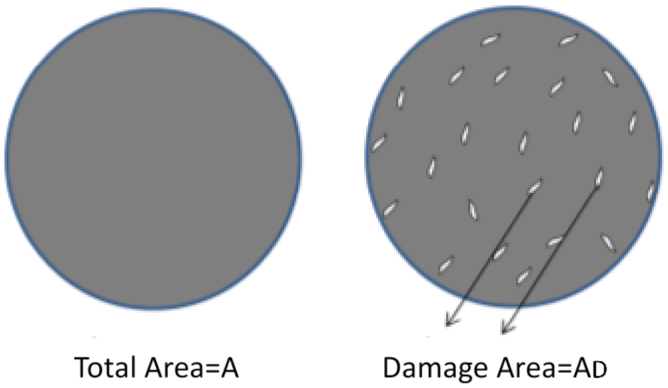

Figure 2 - Material Damage

The degradation is represented by:

$$d = \frac{A_D}{A} \tag{12}$$

Then exist an area that resist efforts known as effective area

$$\bar{A} = A - A_D \tag{13}$$

With eq. 13 is possivel write the damage as:

$$d = 1 - \frac{\bar{A}}{A} \tag{14}$$

If a nominal stresse (σ) and an effective stress ($\bar{\sigma}$) are considered,

$$\sigma = \frac{F}{A} \tag{15}$$

$$\bar{\sigma} = \frac{F}{\bar{A}} \tag{16}$$

then is possible write

$$\frac{\sigma}{\bar{\sigma}} = \frac{A}{\bar{A}} = 1 - d$$
$$\sigma = (1 - d)\bar{\sigma} \tag{17}$$

Damage model is developed in Beserra, 2015

2 STUDY CASES

The formulation in this paper is apply for resolve the hydraulic fracturing problem when exist a natural fracture network.

2.1 Initial stress strain variation

Some simulations were made with the propose of analyzing the influence of initial stress strain in the direction of hydraulic fracturing (pressure propagation) as well as the influence of boundary conditions. Four sceneries were considered. Each one of boundary conditions was tested with an isotropic and anisotropic field of initial stress strain, considering a fluid fracturing rate equal to 1.0E-3 Kg/s. Pre-existing fractures were embedded in finite element mesh with an in-house tool development with properly geological mapping Figure 3.

2.1.1 Hydraulic fracturing with mixed mechanical conditions (slider and fixed)

This first simulation is a field of initial stress strain isotropic. The value from both principal stress is 1MPa (Figure 4(a)). Then a field where maximum stress strain is three times the minimum stress strain was considered. (Figure 4(b)).

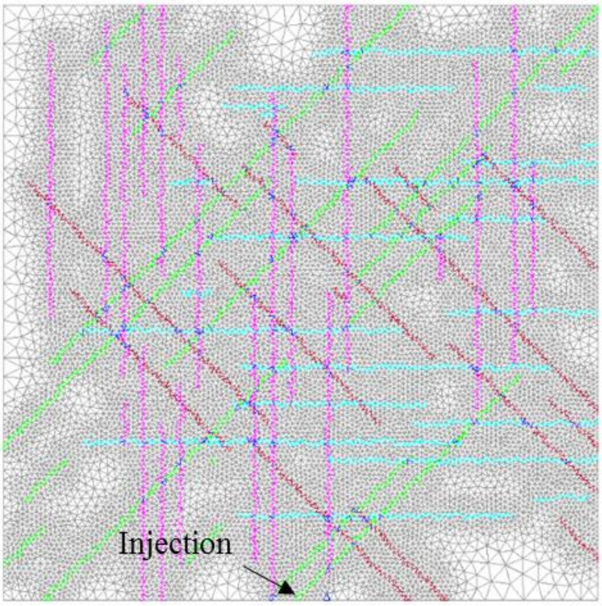

Figure 3.Embedded natural fractures in finite element mesh

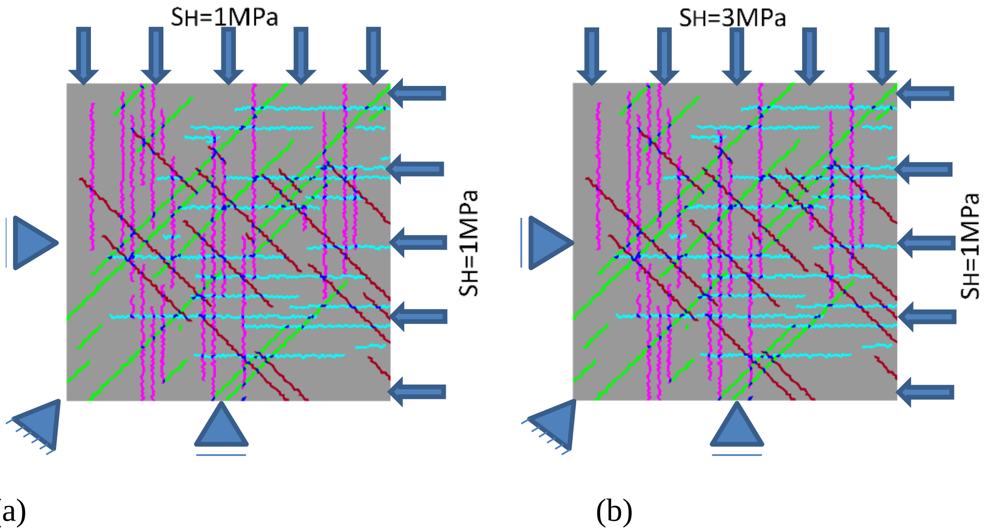

Figure 4. Finite element mesh mixed mechanical conditions. (a) Isotropic stress. (b) Anisotropic stress

As shown in Figure 5, both cases start with a pressure equal to zero.

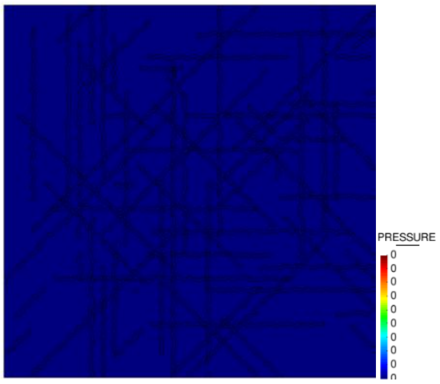

Figure 5. Initial Pressure

The pressure changes throughout the simulation as a function of the fluid injection that is performed Figure 6(a) and Figure 6(b) shown evolution pressure for an isotropic case; Figure 7(a) and Figure 7(b) shown the evolution for an anisotropic case.

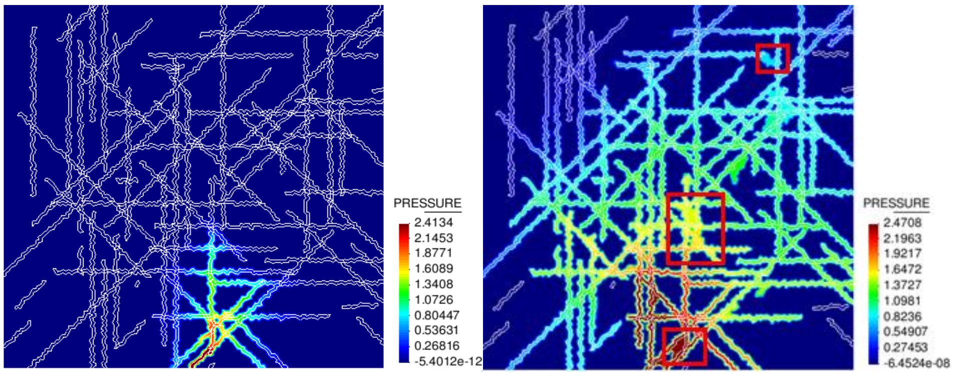

(a) **(b)**

Figure 6.Pressure evolution for hydraulic fracturing operation with isotropic initial stress.

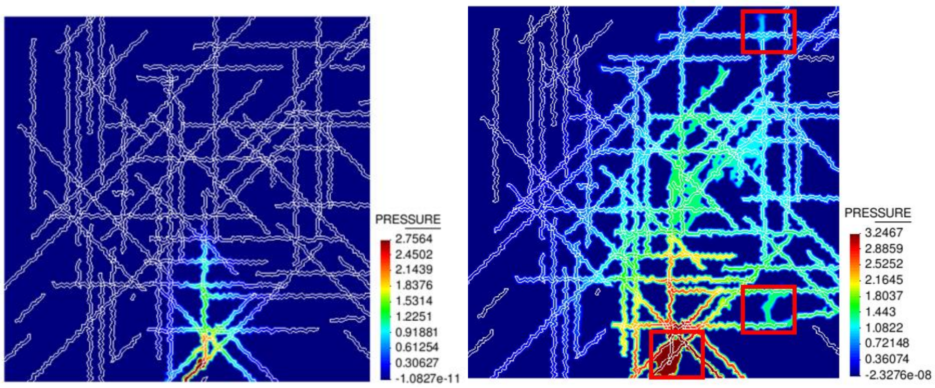

(a) **(b)**

Figure 7.Pressure evolution for hydraulic fracturing operation with anisotropic initial stress.

2.1.2 Hydraulic fracturing with fixed mechanical conditions

A second part the mechanical conditions are fixed throughout the contour, for this, the simulation is fragmented in two parts. First are considered the same mechanical conditions as Figure 4, after a while are considering the condition illustrates in Figure 8 .

As it is presented in the previous case (section 2.1.1), the pressure change during the simulation because of the mechanical boundary conditions and intial stress (Figure 9 and Figure 10) . In order to illustrate clearly de difference between all scenarios are included Figure 11and Figure 12, these figures correspond to normal jump aperture and can be related to the fracture propagation.

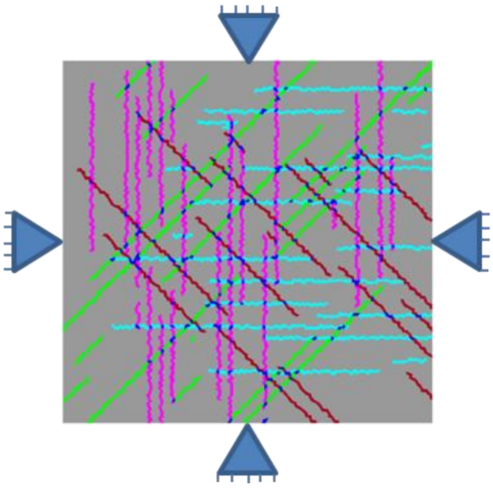

Figure 8.Mechanical boundary conditions for second step.

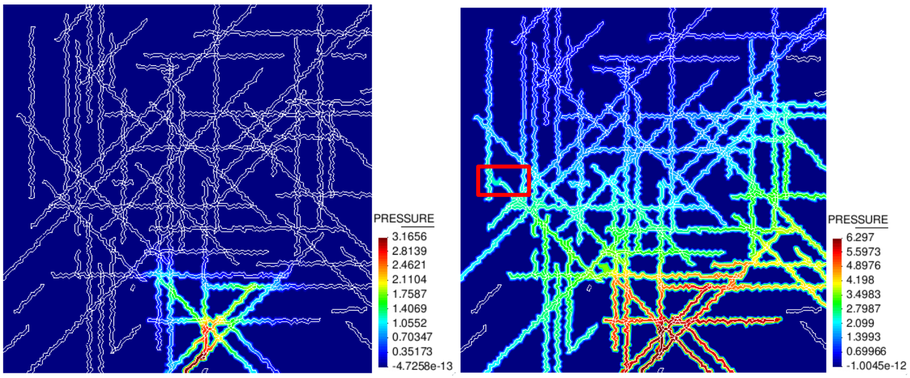

(a) **(b)**

Figure 9.Pressure evolution for hydraulic fracturing operation with isotropic initial stress strain and fixed boundary conditions.

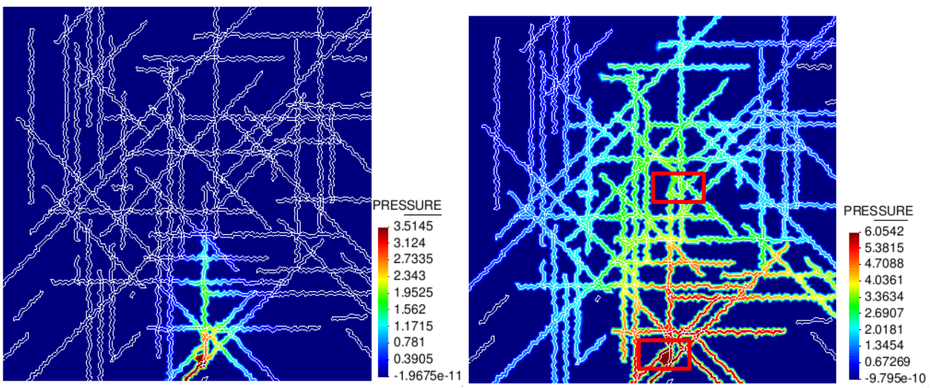

(a) **(b)**

Figure 10. Pressure evolution for hydraulic fracturing operation with anisotropic initial stress strain and fixed boundary conditions.

Proceedings of the XXXVIII Iberian Latin-American Congress on Computational Methods in Engineering
P.O. Faria, R.H. Lopez, L.F.F. Miguel, W.J.S. Gomes, M. Noronha (Editores), ABMEC, Florianópolis, SC, Brazil, November 5-8, 2017.

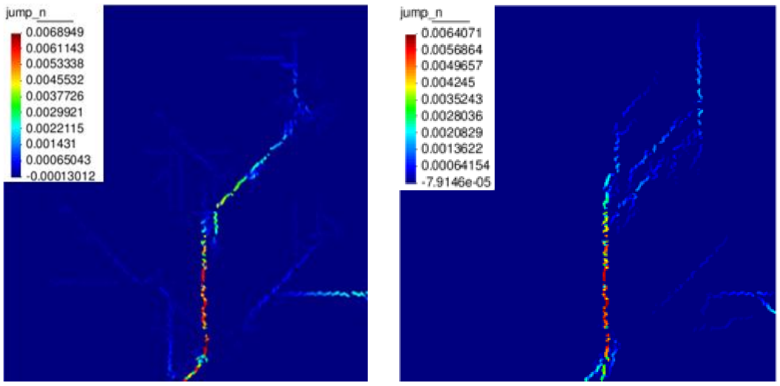

(a) **(b)**

Figure 11. Normal jump aperture. (a) Isotropic stress strain for mixed boundary conditions. (b) Anisotropic Stress strain for mixed boundary conditions.

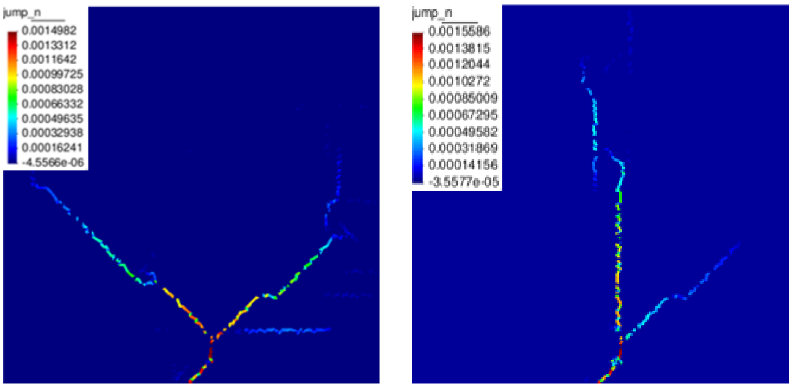

(a) **(b)**

Figure 12. Normal jump aperture. (a) Isotropic stress strain for fixed boundary conditions. (b) Anisotropic Stress strain for fixed boundary conditions

2.2 Well variations

This second case of study was performed to analyze hydraulic fracturing in different scenarios like openhole, perforating and pre-existing fracture. The main objective of this example is to show the effect of the presence of fractures on the propagation of the induced fracture.

The simulations where performed by steps. First, generate the initial stress state prior to the excavation of the well; Second, excavation of formation elements and application of well over pressure (30MPa); finally inject the fracturing fluid. The initial stress state and boundaries conditions are presented in Figure 13. The rock young modulus is 41370 GPa and Poisson 0.2, the fluid fracturing rate used is 1.0 Kg/s. Perforating angles of 30º and 80º were selected to compare fracture evolution in fractured and non fractured reservoir, also were performed combinations of perforating in openhole and casing well. The variable of study is the liquid pressure, which is related with the fracture induced path. The path to the induced fracture will depend on the reservoir conditions in which the hydraulic fracturing operation is performed.

So, for example Figure 14 and Figure 15 shown that for a same time of simulation (10.07 seconds) the pressure of the liquid is in different points of the reservoir.

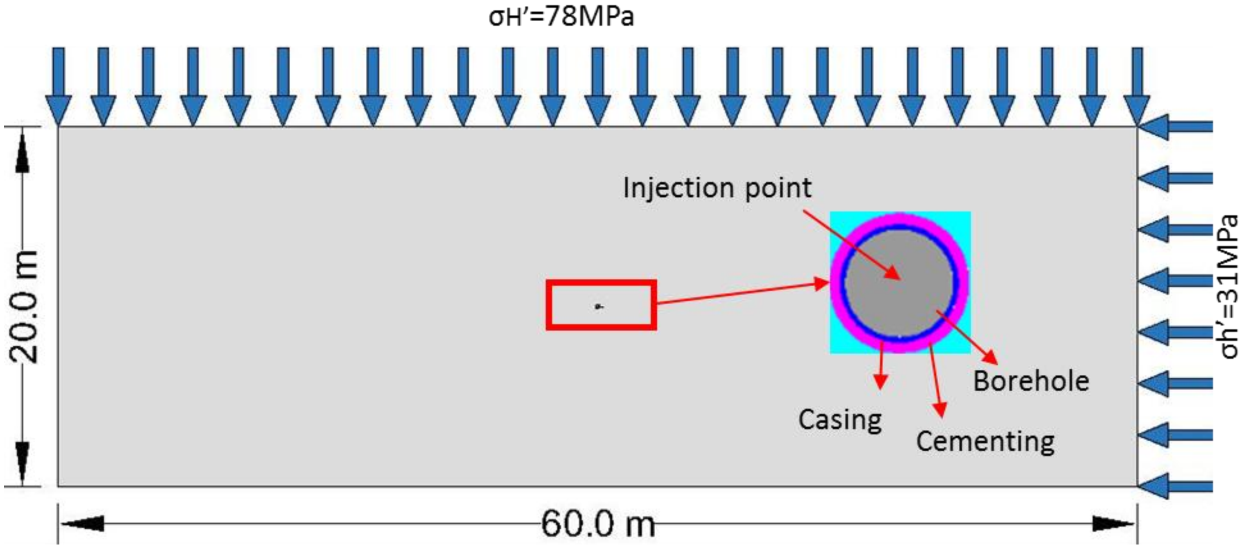

Figure 13 - Well case boundary conditions

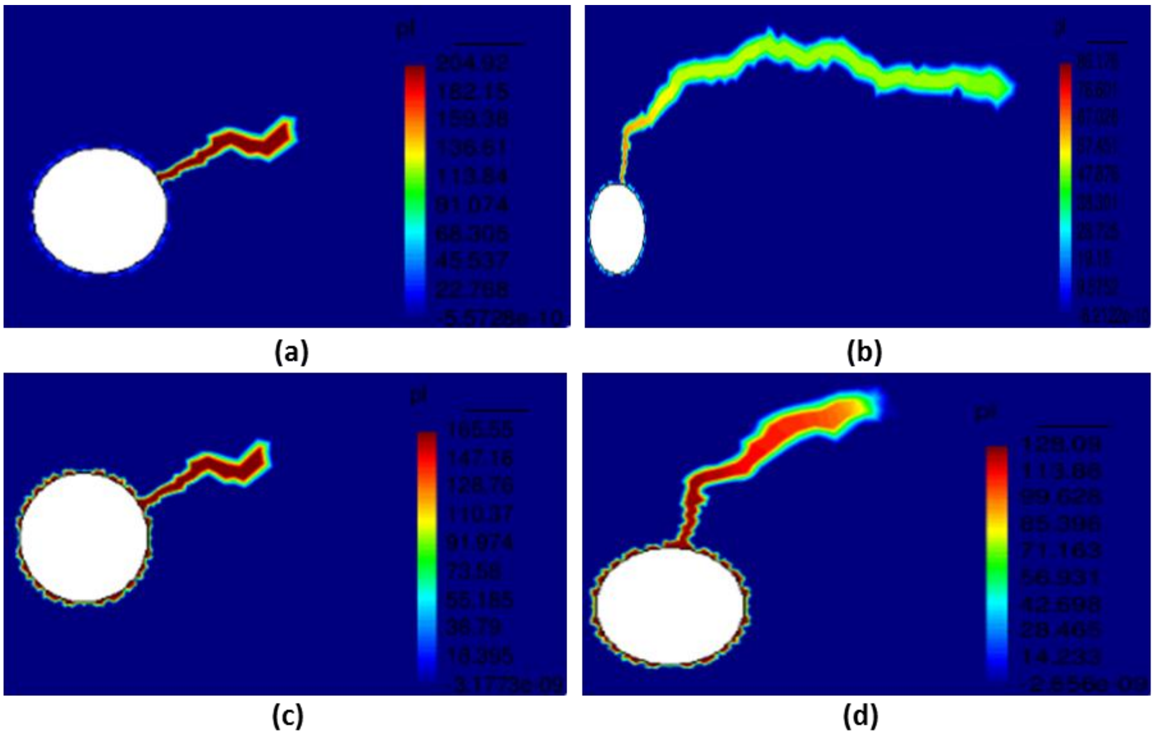

Figure 14 - Pressure at 10.07 seconds in a reservoir without fracture. (a)Well with casing, perforating at 30º.(b) Well with casing, perforating at 80º.(c) Well in openhole, perforating at 30º.(d) Well in openhole, perforating at 80º

Cases in Figure 15 correspond to simulations in a reservoir with pre-existing fractures. In this case liquid pressure goes in the fracture way. It occurs because of the initial stress state and fracture properties while in the homogenous reservoir the pressure tends to go in direction of minimum horizontal stress independent of perforating angle (Figure 14).

Cases that only differ in the presence of a natural fracture present the same slopes but differ in the time of rupture, some cases are only pressurized and fail to advance in the formation. Other cases are propagated through rock matrix (Figure 16). Cases that does not have natural fracture show a typically curve of liquid pressure during a hydraulic fracturing operation (Figure 17), but cases with natural fracture are pressurized (Figure 18).

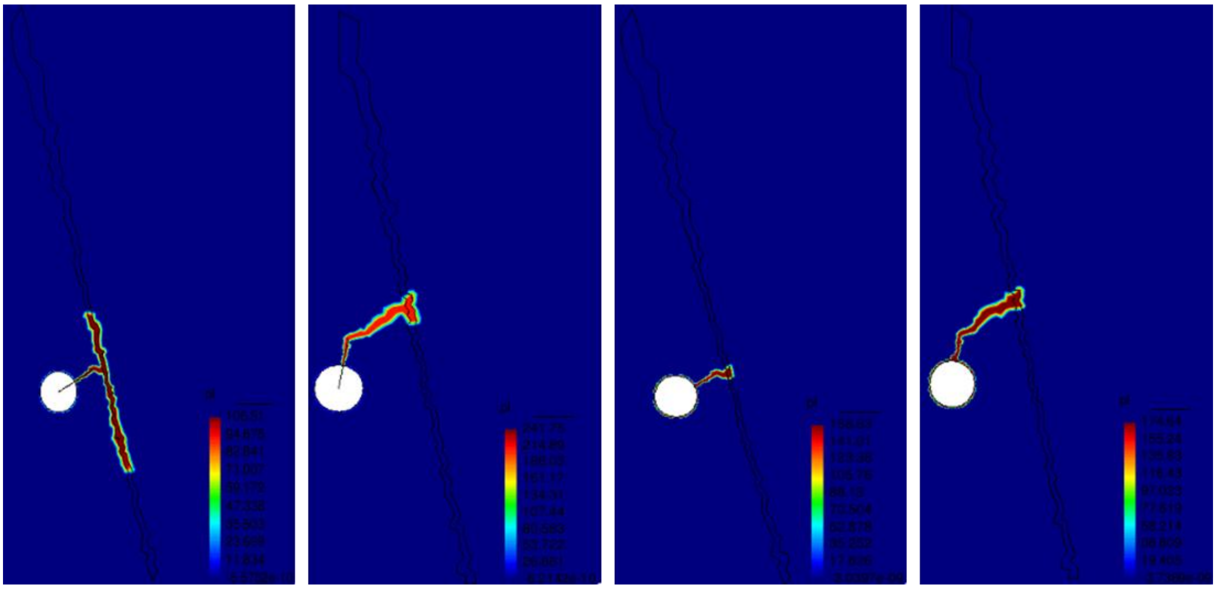

(a) (b) (c) (d)

Figure 15- Pressure at 10.07 seconds in a fractured reservoir.(a)Well with casing, perforating at 30º.(b) Well with casing, perforating at 80º.(c) Well in openhole, perforating at 30º.(d) Well in openhole, perforating at 80º

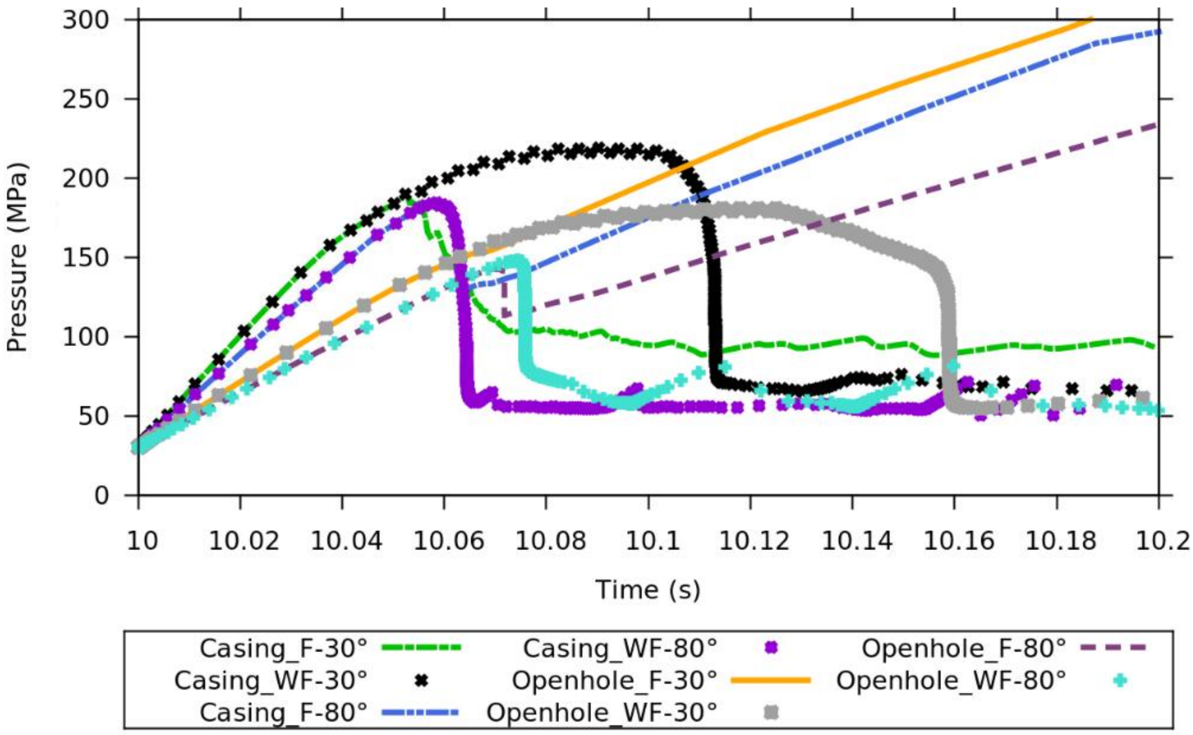

Figure 16 - Liquid Pressure Evolution. F: Pre-existing fracture; WF: Witouth pre-existing fracture

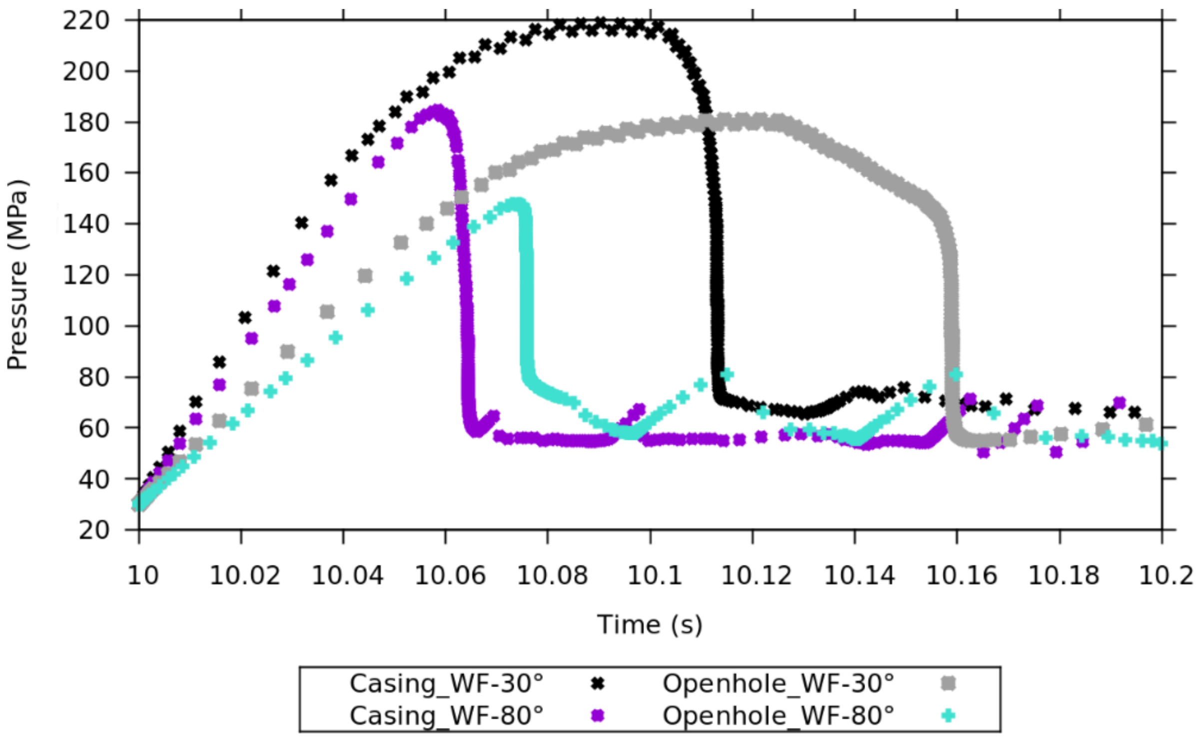

Figure 17 - Liquid pressure evolution. Reservoir naturally unfractured.

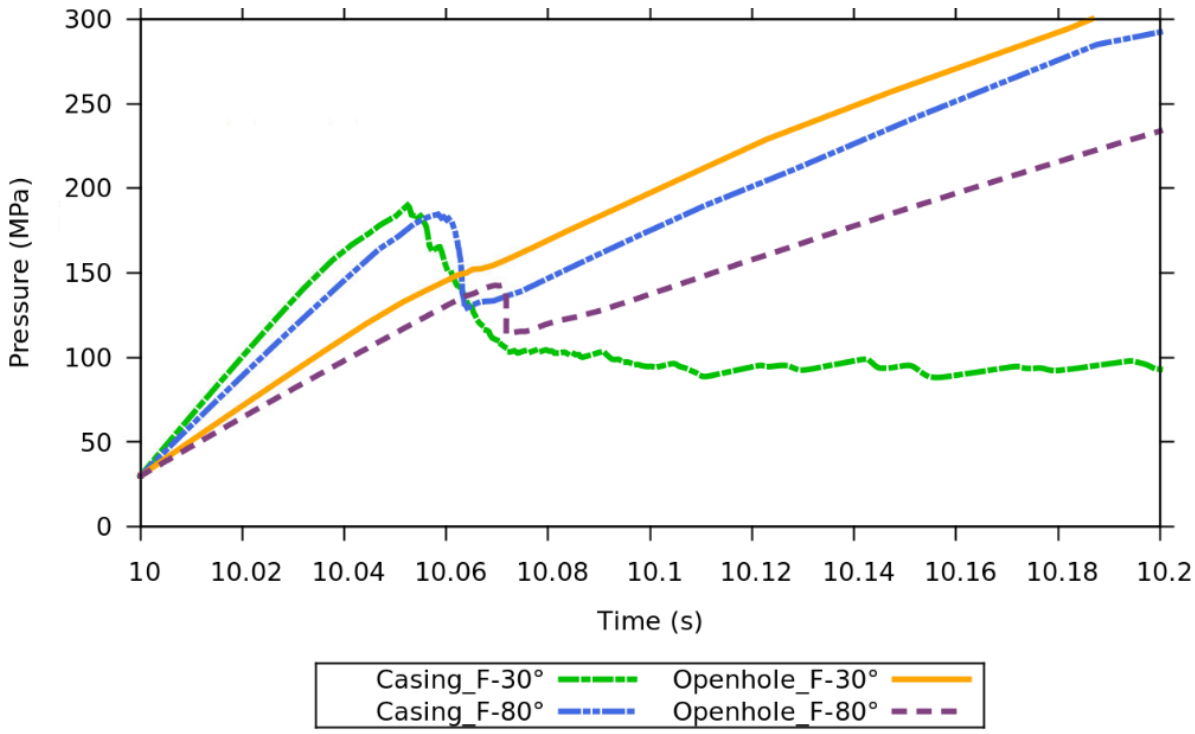

Figure 18 - Liquid pressure evolution. Reservoir naturally fractured.

3 DISCUSSION AND CONCLUSSIONS

In examples where boundaries are fixed the maximum pressure acquired is bigger than examples where exist mixed boundary conditions. It is possible see in the same illustrations, red marks, that due to pressure disturbance caused by hydraulic fracturing the intact rock also undergoes changes.

Rock changes build a connection rock-fracture; that new connections can favor fluid flow due to the increase in reservoir system permeability.

It is also possible to observe the influence that boundary conditions had on the results because the hydraulic fracturing had greater effect on the examples with mixed conditions of contour.

Sometimes the weakness planes are denser in some areas of the reservoir, the degradation of the rock allows to connect fractures that initially were isolated of the zone with greater density.

Cases isotropic does not have a direction for opening fractures, but cases anisotropic open easily in direction of maximum principal stress.

It is necessary to sensitize parameters of the natural fracture to try to know the direction of the induced fracture and known more about fracture intrinsic permeability and stiffness.

ACKNOWLEDGEMENTS

This work has been supported by CAPES/Brazil, EQUION ENERGIA LIMITED and Foundation CMG. Thanks to LMCG for their help and useful discussions.

REFERENCES

Beserra, L. B. de S. (2015). *Análise Hidromecânica do Fraturamento Hidráulico via Elementos Finitos com Descontinuidades Fortes Incorporadas*. Universidade Federal de Pernambuco.

Guimarães, L. D. N., Gens, A., & Olivella, S. (2007). Coupled thermo-hydro-mechanical and chemical analysis of expansive clay subjected to heating and hydration. *Transport in Porous Media*, *66*(3), 341–372. https://doi.org/10.1007/s11242-006-0014-z

Manzoli, O. L. (2011). Predição de propagação de fissuras através de modelos constitutivos locais e técnica de construção progressiva da trajetória de descontinuidade. *Revista Internacional de Metodos Numericos Para Calculo Y Diseno En Ingenieria*, *27*(3), 180–188. https://doi.org/10.1016/j.rimni.2011.07.005

Manzoli, O. L., & Shing, P. B. (2006). A general technique to embed non-uniform discontinuities into standard solid finite elements. *Computers and Structures*, *84*(10–11), 742–757. https://doi.org/10.1016/j.compstruc.2005.10.009

Manzoli, O. L., & Shing, P. B. (2006). A general technique to embed non-uniform discontinuities into standard solid finite elements. *Computers and Structures*, *84*(10–11),

742–757. https://doi.org/10.1016/j.compstruc.2005.10.009

Olivella, S., Gens, A., Carrera, J., & Alonso, E. E. (1996). Numerical formulation for a simulator (CODE_BRIGHT) for the coupled analysis of saline media. *Engineering Computations*, *13*(7), 87–112. https://doi.org/10.1108/02644409610151575

Olivella, S., Carrera, J., Gens, A., & Alonso, E. E. (1994). Nonisothermal multiphase flow of brine and gas through saline media. *Transport in Porous Media*, *15*(3), 271–293. https://doi.org/10.1007/BF00613282

Oliver, J., Huespe, A., & Cante, J. (2008). *An implicit/explicit integration scheme to increase computability of non-linear material and contact/friction problems*. *Computer Methods in Applied Mechanics and Engineering* (Vol. 197). https://doi.org/10.1016/j.cma.2007.11.027